ChemComm

COMMUNICATION

View Article Online
View Journal

Cite this: DOI: 10.1039/c9cc02838b

Received 12th April 2019,
Accepted 17th May 2019

DOI: 10.1039/c9cc02838b

rsc.li/chemcomm

$Ru(TAP)_3^{2+}$ uses multivalent binding to accelerate and constrain photo-adduct formation on DNA†

Willem Vanderlinden, *[ab] Pauline J. Kolbeck,[a] Wout Frederickx,[b] Sebastian F. Konrad,[a] Thomas Nicolaus,[a] Carola Lampe,[a] Alexander S. Urban,[a] Cécile Moucheron[c] and Jan Lipfert[a]

Ru(II)-complexes with polyazaaromatic ligands can undergo direct electron transfer with guanine nucleobases on blue light excitation that results in DNA lesions with phototherapeutic potential. Here we use single molecule approaches to demonstrate DNA binding mode heterogeneity and evaluate how multivalent binding governs the photochemistry of $[Ru(TAP)_3]^{2+}$ (TAP = 1,4,5,8-tetraazaphenanthrene).

Ru(II)-polypyridyl complexes carry three bidentate ligands that can be designed to tune the DNA-binding and electronic properties of the complex.[1,2] Complexes bearing DNA-intercalating moieties can exhibit light-switching properties in the presence of DNA,[3,4] and targeted ligand design has enabled selective detection of mismatches and abasic sites in DNA duplexes.[5,6] Further, π-deficient ligands such as polyazaaromatic TAP (1,4,5,8-tetraazapenanthrene) convey highly oxidizing properties to the complex in the triplet metal-to-ligand charge transfer (^{3}MLCT) excited state: on excitation, the homoleptic complex **$Ru(TAP)_3^{2+}$** (Fig. 1) can extract an electron from guanine nucleobases.[7] The oxidized guanine either undergoes a back-electron transfer with the reduced complex or results in DNA-lesions. While the formation of single-strand DNA breaks is easily detected *via* topological conversions of supercoiled DNA targets, recombination of the oxidized guanine with the reduced complex to form covalent photo-adducts[8] is the dominant pathway. Recent work has demonstrated targeted photo-induced DNA damage by Ru–TAP complexes in live cells,[9] suggesting that this class of compounds could be used in phototherapeutic applications.

To design Ru–TAP complexes for therapeutic applications, it is essential to understand how ground-state DNA-binding affects the photochemistry of **$Ru(TAP)_3^{2+}$** with DNA. However, the binding mode of **$Ru(TAP)_3^{2+}$** and the related **$Ru(phen)_3^{2+}$** (phen = 1,10-phenanthroline; Fig. 1) to DNA is controversial, with evidence for (hydrogen bond-mediated[10]) groove-binding as well as binding through intercalation[11] or semi-intercalation, *i.e.* partial insertion between adjacent basepairs.[12–15] Here, we use

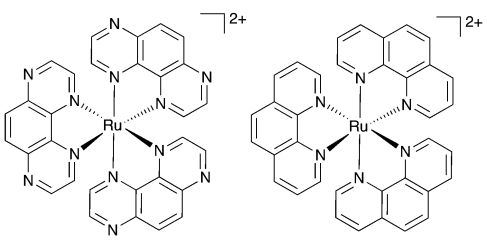

Fig. 1 Chemical structures of **$Ru(TAP)_3^{2+}$** (left) and **$Ru(phen)_3^{2+}$** (right).

[a] Department of Physics, Nanosystems Initiative Munich, and Center for NanoScience, LMU Munich, Amalienstrasse 54, 80799 Munich, Germany
[b] Department of Chemistry, Division of Molecular Imaging and Photonics, KU Leuven-University of Leuven, Celestijnenlaan 200F, B-3001 Leuven, Belgium. E-mail: willem.vanderlinden@kuleuven.be
[c] Department of Chemistry, Laboratory of Organic Chemistry and Photochemistry, Université Libre de Bruxelles, Avenue Franklin D. Roosevelt 50, 1050 Brussels, Belgium

† Electronic supplementary information (ESI) available: Methods section, supporting Fig. S1 and S2. See DOI: 10.1039/c9cc02838b

Willem Vanderlinden

Willem Vanderlinden obtained his PhD under the supervision of Steven De Feyter (Department of Chemistry, KU Leuven, Belgium) using atomic force microscopy to image and quantify interactions of DNA with proteins and small molecules. Afterwards, he moved to Germany as a postdoctoral fellow of the FWO-Flanders to join the lab of Jan Lipfert (Physics Department, LMU Munich) where he developed magnetic tweezers assays to study the dynamics of retroviral integration and DNA supercoiling. Within the same laboratory, he is currently a junior group leader unravelling how nucleic acids are (re-)arranged in the context of multipart nucleoprotein complexes.

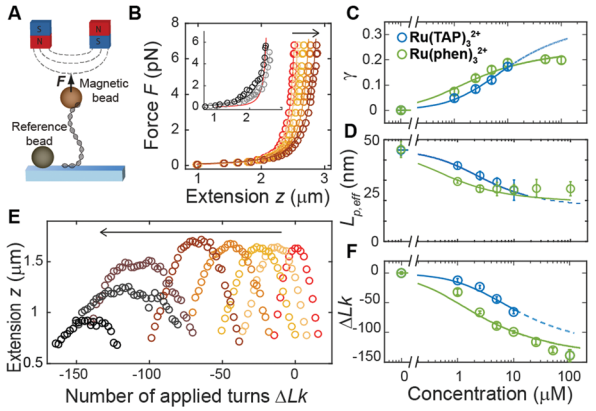

Fig. 2 Magnetic tweezers probe DNA structural changes on binding **Ru(TAP)$_3^{2+}$** and **Ru(phen)$_3^{2+}$**. (A) Schematic representation of DNA in MT. (B) Force-extension analysis of DNA in the absence (red) and presence (brown gradient) of increasing concentrations (1–10 μM) of **Ru(TAP)$_3^{2+}$**. Inset: Anomalous force-extension behaviour at high (50 and 100 μM) ligand concentration. Solid lines are WLC fits to the data. (C) Fractional occupancy γ as function of C(**Ru(TAP)$_3^{2+}$**) (blue) and C(**Ru(phen)$_3^{2+}$**) (green) and fits to the McGhee-von Hippel model with (K_D = 19.7 ± 4 μM, n = 2.7 ± 0.4) and (K_D = 4.9 ± 1 μM, n = 4.0 ± 0.2) for **Ru(TAP)$_3^{2+}$** and **Ru(phen)$_3^{2+}$** respectively. (D) Effective bending persistence length as a function of C(**Ru(TAP)$_3^{2+}$**) (blue) and C(**Ru(phen)$_3^{2+}$**) (green) and fit to the Popov model. (E) Rotation curves of DNA in the absence (red) and presence (brown gradient) of increasing concentrations (1–100 μM) of **Ru(TAP)$_3^{2+}$**. (F) Shift of the centre position of rotation curves as a function of C(**Ru(TAP)$_3^{2+}$**) (blue) and C(**Ru(phen)$_3^{2+}$**) (green). Solid lines are fits to the McGhee-von Hippel model taking (K,n) from the lengthening data. The fitted unwinding angles are ϕ = 16 ± 4° for **Ru(TAP)$_3^{2+}$** and ϕ = 26 ± 2° for **Ru(phen)$_3^{2+}$**.

single-molecule approaches to unravel the binding modes of racemic **Ru(TAP)$_3^{2+}$** and show how they affect the photochemistry with DNA.

Previously, single-molecule manipulation assays have revealed the binding modes of small molecules interacting with DNA.[16–20] We use magnetic tweezers (MT) to quantify the ground-state binding of racemic **Ru(TAP)$_3^{2+}$** and **Ru(phen)$_3^{2+}$** to DNA in 10 mM phosphate buffer (Fig. 2A). In MT, DNA molecules (7.95 kbp; crystallographic length 2.7 μm) were attached at one end to the bottom surface of a flow cell and at the other end to a paramagnetic bead. Using permanent magnets, we can controllably exert stretching forces and torques[21] on the DNA molecules.

First, we performed force-extension measurements on nicked DNA tethers to evaluate the changes in DNA extension and elasticity on titration with racemic **Ru(TAP)$_3^{2+}$** (Fig. 2B). By fitting the worm-like chain (WLC) model,[22] we determined the DNA contour length L_c and bending persistence length L_p. In the absence of **Ru(TAP)$_3^{2+}$** we find L_c = 2.68 ± 0.03 μm and L_p = 45 ± 3 nm, in excellent agreement with the crystallographic length of B-form DNA and with previous measurements of L_p, respectively.[23] On addition of low to intermediate concentrations ([**Ru(TAP)$_3^{2+}$**] ≤ 10 μM), L_c increases gradually, while L_p decreases (Fig. 2C and D). The increase of L_c is consistent with intercalative binding, and can be used to calculate the fractional occupancy γ of intercalated **Ru(TAP)$_3^{2+}$** *via* $\gamma = (L_C(C) - L_c(0))/(\Delta l \cdot N)$ with $L_c(0)$ the contour length in the absence of **Ru(TAP)$_3^{2+}$**, Δl the contour length increment per intercalation event, and N the number of basepairs (7.95 kbp).[17]

Assuming Δl = 0.34 nm, we fit the **Ru(TAP)$_3^{2+}$** data to the McGhee-von Hippel model:[24]

$$\gamma_{(C)} = \frac{[\mathbf{Ru(TAP)_3^{2+}}]}{K_D} \cdot \frac{(1-n\gamma)^n}{(1-n\gamma+\gamma)^{n-1}}$$

and obtain the dissociation constant K_D = 19.7 ± 4 μM and binding site size n = 2.7 ± 0.4 (Fig. 2C). While lengthening of the DNA contour is consistent with an intercalative binding mode, linear dichroism experiments[12] and crystallographic data[13] have suggested semi-intercalation, *i.e.* partial insertion of a TAP ligand between subsequent basepairs. Co-crystal structures of DNA and TAP-containing (but heteroleptic) Ru(II)-complexes further feature a sharp kink (with bend angle θ = 51°) in the DNA at the semi-intercalation binding pocket of the complex.[13] We tested whether the dependency of the effective bending persistence length $L_{p,eff}$ on [**Ru(TAP)$_3^{2+}$**] can be described by the model of Popov *et al.*[26] that features a line density κ of rigid bends with bend angle θ:

$$L_{p,eff} = \frac{L_{p,0}}{1 + \kappa L_{p,0}(1-\cos\theta)}$$

Fixing K_D = 19.7 μM and n = 2.7 (determined from the contour length increase), we obtain a kink angle θ = 11° (Fig. 2D), far below the value suggested by crystallography.[13] Conversely, fixing θ = 51°, we obtain a best fit with a kink frequency that is ≈10-fold smaller than the fractional occupancy of intercalated **Ru(TAP)$_3^{2+}$** γ. Thus, our data are inconsistent with the view that TAP predominantly interacts with DNA *via* semi-intercalation that results in severe DNA kinking.

We note that at [**Ru(TAP)$_3^{2+}$**] > 10 μM the WLC model does not provide a good fit to the force-extension data and that the DNA length decreases with increasing concentration, suggesting effects of **Ru(TAP)$_3^{2+}$** binding beyond intercalation. In contrast, the force-extension behaviour of DNA interacting with racemic **Ru(phen)$_3^{2+}$** is accurately described by the WLC model over the entire concentration range tested (0–100 μM) and we find K_D = 4.9 ± 1 μM, n = 4.0 ± 0.2 fitting the McGhee-von Hippel equation (Fig. 2C). Similar to **Ru(TAP)$_3^{2+}$**, **Ru(phen)$_3^{2+}$**-binding decreases the DNA bending persistence length $L_{p,eff}$, and fitting the Popov model[26] yields a kink density $\kappa = 0.12 \cdot \gamma / 0.34$ nm (for θ = 51°) (Fig. 2D).

To obtain additional insights in the binding of **Ru(TAP)$_3^{2+}$** with DNA, we use the capability of MT to control the DNA linking number Lk in torsionally constrained DNA by rotating the external magnets. At low force (F = 0.3 pN) magnet rotation leads to a symmetrical response of the molecular extension for both under- and over-winding of bare DNA, due to the formation of plectonemic supercoils[21] (Fig. 2E). Titration with **Ru(TAP)$_3^{2+}$** induces a shift of the midpoints of the rotation curves to more negative linking differences ΔLk, in line with DNA unwinding upon **Ru(TAP)$_3^{2+}$** intercalation[16] (Fig. 2E). Using K_D and n from the force-extension data (Fig. 2B and C), we determined the unwinding angle ϕ = 16 ± 4° per intercalation event from the dependence of ΔLk on [**Ru(TAP)$_3^{2+}$**] (Fig. 2F). Notably, at [**Ru(TAP)$_3^{2+}$**] > 10 μM the extension of the rotation curves rapidly decreases with increasing concentration, in contrast to the behaviour for classical intercalation, but in agreement with the observations from force-extension experiments.

Notably, at these higher concentrations, the rotation curves become more erratic and feature sudden extension jumps.

In contrast, rotation curves with increasing concentrations of **Ru(phen)$_3^{2+}$** follow the behaviour of a classical intercalator (Fig. S1, ESI†). Analysis of the shift in ΔLk yields an unwinding angle $\phi = 26.3 \pm 2^\circ$ for **Ru(phen)$_3^{2+}$** (Fig. 2E and F), in reasonable agreement with the results of a topoisomerase assay.[27] Together, our data indicate that **Ru(phen)$_3^{2+}$** is a stronger intercalator than **Ru(TAP)$_3^{2+}$**, in agreement with a previous report.[28] We note that for **Ru(phen)$_3^{2+}$** only at high [**Ru(phen)$_3^{2+}$**] = 100 μM, and in few cases (~10% of all beads), the maximal extension in rotation curves is reduced with respect to the expected values, in contrast to the anomalous behaviour observed for **Ru(TAP)$_3^{2+}$**.

To dynamically probe the anomalous behaviour at [**Ru(TAP)$_3^{2+}$**] > 10 μM we subjected nicked DNA tethers to rotation in the MT (Fig. S2A, ESI†). At low concentrations (<10 μM), tether extension remains unaffected on magnet rotation, as expected for a torsionally unconstrained DNA. However, at [**Ru(TAP)$_3^{2+}$**] > 10 μM, the DNA extension occasionally decreases on magnet rotation until sudden extension jumps restore the original z-position. We interpret this result as the consequence of topological shielding of the nicking site *via* transient DNA looping by binding to multiple sites that bridge the nick. To further test the hypothesis of DNA looping by **Ru(TAP)$_3^{2+}$** we performed force-jump experiments wherein the DNA is first kept at a low force (0.1 pN) and then suddenly subjected to a high force (6 pN). In the presence of [**Ru(TAP)$_3^{2+}$**] > 10 μM, our data demonstrate step-wise extension increments on application of high force, in line with forced dissociation of **Ru(TAP)$_3^{2+}$**-mediated loops (Fig. S2B, ESI†). Consistent with our observations of classical intercalation (Fig. 2), no signatures for **Ru(phen)$_3^{2+}$**-mediated loop formation were observed from force-jump experiments or rotation of nicked DNA.

To directly visualize the bending or kinking behaviour at short length scales, we performed atomic force microscopy (AFM) imaging. Linear DNA fragments (486 bp) were incubated with **Ru(TAP)$_3^{2+}$** under dimmed light conditions and subsequently deposited onto poly-L-lysine coated mica (Methods). We analysed the AFM images by tracing the DNA contour[29] with a step length $\ell = 5$ nm. Under the conditions used, we find that at the molecular length scale DNA adopts conformations corresponding to kinetic trapping on surface adsorption, as observed previously.[25] Yet, at short length scales ($\ell = 5$ nm) the bend angle distribution implies local chain equilibration that enables quantitative evaluation of DNA bending or kinking (if any) on incubation with **Ru(TAP)$_3^{2+}$**. The bend angle distributions of DNA molecules incubated with varying amounts of **Ru(TAP)$_3^{2+}$** are, to first approximation, well described by a single folded Gaussian (Fig. 3B) with a variance $\langle\theta^2\rangle$ that relates to the DNA persistence length as $\langle\theta^2\rangle = \ell/L_p$. Based on this analysis, we only find a weak dependence of L_p on [**Ru(TAP)$_3^{2+}$**]. On average $L_p = 58 \pm 3$ nm in agreement with previous AFM analyses of DNA bending behaviour.[29] However, the fit residuals feature a peak at angles of 40–50°, in a concentration-dependent fashion. The integrated peak accounts only for ≈1.5% of the total angle distribution at the highest concentrations tested in good agreement with our MT analysis that suggests infrequent kinks induced by **Ru(TAP)$_3^{2+}$**.

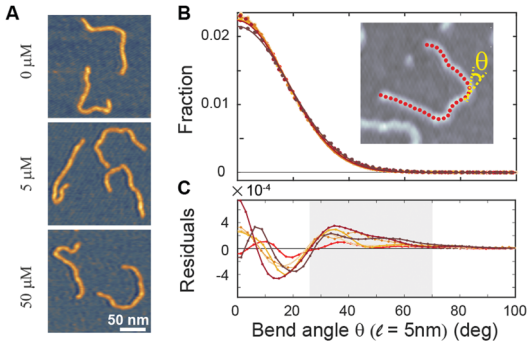

Fig. 3 Atomic force microscopy demonstrates **Ru(TAP)$_3^{2+}$**-mediated DNA kinking with low yield. (A) AFM topographs of 486 bp linear DNA molecules incubated with increasing concentrations of **Ru(TAP)$_3^{2+}$**. (B) Bend angle distributions (Kernel density estimate with bandwidth 4°) of DNA generated by automated tracing of the chain contours with a step length $\ell = 5$ nm. For each condition ≈10 000 angles are recorded. Solid lines are fits to a folded Gaussian. Colour code is the same as in Fig. 2. (C) Residuals of the folded Gaussian fits in (B) depicting a concentration-dependent increase of bend angles in the range of 30 deg < θ < 70 deg (grey area).

Taken together, our MT and AFM data suggest that **Ru(TAP)$_3^{2+}$** binds to DNA in an intercalative binding mode that occasionally forms kinks and that infers helix lengthening and unwinding. In addition, we observe clear evidence for binding-induced loop formation that implies multivalent binding to DNA, which in turn suggests that **Ru(TAP)$_3^{2+}$** can interact *via* (at least) two interfaces simultaneously. Interestingly, **Ru(phen)$_3^{2+}$** does not form DNA synapses to the extent observed for **Ru(TAP)$_3^{2+}$**, despite the higher affinity for intercalation, suggesting that loop formation is mediated in part by the N1 and N8 atoms of TAP, potentially *via* hydrogen bonding.[10]

To address how multivalent binding by **Ru(TAP)$_3^{2+}$** might impact excited state processes, we carried out spectroscopic measurements with either short (32 bp; 50% GC; expected to behave as a rigid rod) or long (48501 bp; 49% GC; that will adopt a random coil conformation, which increases the local concentration of DNA segments) DNA to modulate the contact probability that would lead to **Ru(TAP)$_3^{2+}$**-mediated synapse formation. First we tested whether DNA length affects luminescence by recording spectra upon titrating **Ru(TAP)$_3^{2+}$** (5 μM) with the different DNA substrates. Luminescence quenching was evaluated for both DNA substrates in the same concentration range ([bp] = 0–250 μM) and found to be approximately independent of DNA length (Fig. 4A and B). The quenching as a function of [bp] is well-described by the McGhee-von Hippel binding model with (K_D,n) from the force-extension data and including an offset that takes into account non-productive binding at AT-sequences. The luminescence quenching follows the same concentration dependence as the lengthening observed in MT, which strongly suggests that intercalative binding governs quenching of the ^{3}MLCT state.

To probe the effect of local DNA concentration on photoadduct formation, we recorded the changes in absorption at the MLCT bands on irradiation of **Ru(TAP)$_3^{2+}$** (5 μM) at 465 nm, in the presence of either 32 bp or 48.5 kbp-long DNA ([bp] = 100 μM;

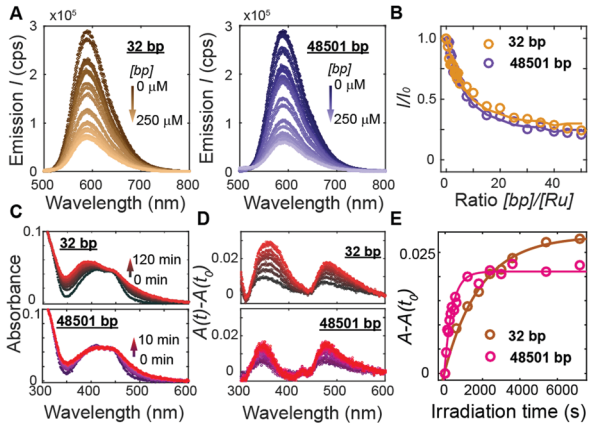

Fig. 4 DNA length-dependence of excited state processes in **Ru(TAP)$_3^{2+}$**. (A) Photoluminescence ($\lambda_{excitation}$ = 436 nm) of **Ru(TAP)$_3^{2+}$** (5 μM) on titration with DNA. Left: Titration with 32 bp DNA ([bp] = 0–250 μM; brown gradient). Right: Titration with 48.5 kbp DNA ([bp] = 0–250 μM; violet gradient). (B) Normalized luminescence intensity ($\lambda_{emission}$ = 590 nm) as a function of bp-to-Ru^{2+} concentration ratio. Solid lines are fits to the McGhee-von Hippel equation, using K_D and n obtained from MT data and a variable plateau value that accounts for unproductive binding. (C) Absorbance spectra of **Ru(TAP)$_3^{2+}$** (5 μM) in the presence of DNA ([bp] = 100 μM) after irradiation at 465 nm for different irradiation times. Top: Absorbance spectra on irradiation in the presence of 32 bp DNA. Bottom: Spectra obtained on irradiation in the presence of 48.5 kbp DNA. (D) Difference absorption spectra for different irradiation times with respect to absorbance prior to irradiation ($t = t_0$). (E) Difference absorption at 350 nm as a function of irradiation time in mixtures containing 5 μM **Ru(TAP)$_3^{2+}$** and either 32 bp or 48501 bp DNA ([bp] = 100 μM). Solid lines are fits to first-order kinetics, with reaction lifetimes $\tau = 33 \pm 7$ min and $\tau = 7 \pm 2$ min for photoadduct formation on 32 bp and 48.5 kbp DNA, respectively.

Fig. 4C and D). Formation of covalent adducts leads to the appearance of an absorption peak at ≈350 nm whereas non-covalent adducts resulting from ligand-exchange with a nucleobase increase the absorption at ≈500 nm.[30] We find that photo-adduct formation is faster for the long than for the short DNA (with first order reaction times of $\tau = 7 \pm 2$ min and $\tau = 33 \pm 7$ min, respectively; Fig. 4E), but achieves a lower final yield. In addition, the peak at 350 nm is much narrower for the long DNA construct as compared the short variant (Fig. 4D), implying a smaller range of photo-adduct species. The spectroscopic data demonstrate that photo-adduct formation, in contrast to luminescence quenching, is faster on long than on short DNA. The lower yield and better-defined photo-adducts suggest that binding to long DNA imposes geometrical constraints that prevent the formation of a broad range of products.

In conclusion, our work reconciles previous apparently contradicting reports on the DNA-binding modes of **Ru(TAP)$_3^{2+}$**. Racemic **Ru(TAP)$_3^{2+}$** and **Ru(phen)$_3^{2+}$** can interact with DNA *via* (semi-)intercalation that occasionally occurs in a kinked state, consistent with a combination of the differential effects observed for enantiopure complexes.[11–15] **Ru(TAP)$_3^{2+}$** additionally can mediate DNA looping, presumably *via* combined (semi-)intercalation and hydrogen-bonding.[10] This multivalent binding might explain the differential yield of photo-adduct formation on short *versus* long DNA. The dependence of photo-adduct formation on local DNA concentration is important towards applications of Ru–TAP complexes *in vivo*.

We thank the Deutsche Forschungsgemeinschaft (SFB 863, project A11) and F.R.S-F.N.R.S. (CDR J.0022.18) for funding, and Theo Lohmueller and Stefanie Pritzl for use of a LED.

Conflicts of interest

There are no conflicts to declare.

References

1 F. E. Poynton, S. A. Bright, S. Blasco, D. C. Williams, J. M. Kelly and T. Gunnlaugsson, *Chem. Soc. Rev.*, 2017, **46**, 7706–7756.
2 F. Heinemann, J. Karges and G. Gasser, *Acc. Chem. Res.*, 2017, **50**, 2727–2736.
3 A. E. Friedman, J. C. Chambron, J. P. Sauvage, N. J. Turro and J. K. Barton, *J. Am. Chem. Soc.*, 1990, **112**, 4960–4962.
4 C. Moucheron, A. Kirsch-De Mesmaeker and S. Choua, *Inorg. Chem.*, 1997, **36**, 584–592.
5 A. N. Boynton, L. Marcélis and J. K. Barton, *J. Am. Chem. Soc.*, 2016, **138**, 5020–5023.
6 Q. Deraedt, L. Marcélis, F. Loiseau and B. Elias, *Inorg. Chem. Front.*, 2017, **4**, 91–103.
7 J.-P. Lecomte, A. K.-D. Mesmaeker, J. M. Kelly, A. B. Tossi and H. Görner, *Photochem. Photobiol.*, 1992, **55**, 681–689.
8 L. Jacquet, R. J. H. Davies, A. Kirsch-De Mesmaeker and J. M. Kelly, *J. Am. Chem. Soc.*, 1997, **119**, 11763–11768.
9 C. S. Burke, A. Byrne and T. E. Keyes, *J. Am. Chem. Soc.*, 2018, **140**, 6945–6955.
10 W. Vanderlinden, M. Blunt, C. C. David, C. Moucheron, A. Kirsch-De Mesmaeker and S. De Feyter, *J. Am. Chem. Soc.*, 2012, **134**, 10214–10221.
11 J. K. Barton, A. Danishefsky and J. Goldberg, *J. Am. Chem. Soc.*, 1984, **106**, 2172–2176.
12 P. Lincoln and B. Nordén, *J. Phys. Chem. B*, 1998, **102**, 9583–9594.
13 J. P. Hall, K. O'Sullivan, A. Naseer, J. A. Smith, J. M. Kelly and C. J. Cardin, *Proc. Natl. Acad. Sci. U. S. A.*, 2011, **108**, 17610.
14 S. Satyanarayana, J. C. Dabrowiak and J. B. Chaires, *Biochemistry*, 1992, **31**, 9319–9324.
15 K. Gisselfält, P. Lincoln, B. Nordén and M. Jonsson, *J. Phys. Chem. B*, 2000, **104**, 3651–3659.
16 J. Lipfert, S. Klijnhout and N. H. Dekker, *Nucleic Acids Res.*, 2010, **38**, 7122–7132.
17 I. D. Vladescu, M. J. McCauley, M. E. Nuñez, I. Rouzina and M. C. Williams, *Nat. Methods*, 2007, **4**, 517.
18 M. Manosas, J. Camunas-Soler, V. Croquette and F. Ritort, *Nat. Commun.*, 2017, **8**, 304.
19 K. Günther, M. Mertig and R. Seidel, *Nucleic Acids Res.*, 2010, **38**, 6526–6532.
20 A. Sischka, K. Toensing, R. Eckel, S. D. Wilking, N. Sewald, R. Ros and D. Anselmetti, *Biophys. J.*, 2005, **88**, 404–411.
21 T. R. Strick, J. F. Allemand, D. Bensimon, A. Bensimon and V. Croquette, *Science*, 1996, **271**, 1835.
22 C. Bouchiat, M. D. Wang, J. F. Allemand, T. Strick, S. M. Block and V. Croquette, *Biophys. J.*, 1999, **76**, 409–413.
23 F. Kriegel, N. Ermann and J. Lipfert, *J. Struct. Biol.*, 2017, **197**, 26–36.
24 J. D. McGhee and P. H. von Hippel, *J. Mol. Biol.*, 1974, **86**, 469–489.
25 T. Brouns, H. De Keersmaecker, S. F. Konrad, N. Kodera, T. Ando, J. Lipfert, S. De Feyter and W. Vanderlinden, *ACS Nano*, 2018, **12**, 11907–11916.
26 Y. O. Popov and A. V. Tkachenko, *Phys. Rev. E: Stat., Nonlinear, Soft Matter Phys.*, 2005, **71**, 051905.
27 J. M. Kelly, A. B. Tossi, D. J. McConnell and C. OhUigin, *Nucleic Acids Res.*, 1985, **13**, 6017–6034.
28 A. B. Tossi and J. M. Kelly, *Photochem. Photobiol.*, 1989, **49**, 545–556.
29 P. A. Wiggins, T. van der Heijden, F. Moreno-Herrero, A. Spakowitz, R. Phillips, J. Widom, C. Dekker and P. C. Nelson, *Nat. Nanotechnol.*, 2006, **1**, 137.
30 M. M. Feeney, J. M. Kelly, A. B. Tossi, A. K.-d. Mesmaeker and J.-P. Lecomte, *J. Photochem. Photobiol., B*, 1994, **23**, 69–78.

